UNIVERSITY OF WEST LONDON
The Career University

UWL REPOSITORY

repository.uwl.ac.uk

Towards efficient structural and serviceability design of high-strength concrete t-beams

Shaaban, Ibrahim ORCID logoORCID: https://orcid.org/0000-0003-4051-341X and Mustafa, Tarek S. (2021) Towards efficient structural and serviceability design of high-strength concrete t-beams. Proceedings of the Institution of Civil Engineers - Structures and Buildings, 174 (10). pp. 836-848. ISSN 0965-0911

http://dx.doi.org/10.1680/jstbu.19.00081

This is the Accepted Version of the final output.

UWL repository link: https://repository.uwl.ac.uk/id/eprint/6314/

Alternative formats: If you require this document in an alternative format, please contact: open.research@uwl.ac.uk

Copyright:

Copyright and moral rights for the publications made accessible in the public portal are retained by the authors and/or other copyright owners and it is a condition of accessing publications that users recognise and abide by the legal requirements associated with these rights.

Take down policy: If you believe that this document breaches copyright, please contact us at open.research@uwl.ac.uk providing details, and we will remove access to the work immediately and investigate your claim.

Accepted manuscript doi:
10.1680/jstbu.19.00081

Accepted manuscript
As a service to our authors and readers, we are putting peer-reviewed accepted manuscripts (AM) online, in the Ahead of Print section of each journal web page, shortly after acceptance.

Disclaimer
The AM is yet to be copyedited and formatted in journal house style but can still be read and referenced by quoting its unique reference number, the digital object identifier (DOI). Once the AM has been typeset, an 'uncorrected proof' PDF will replace the 'accepted manuscript' PDF. These formatted articles may still be corrected by the authors. During the Production process, errors may be discovered which could affect the content, and all legal disclaimers that apply to the journal relate to these versions also.

Version of record
The final edited article will be published in PDF and HTML and will contain all author corrections and is considered the version of record. Authors wishing to reference an article published Ahead of Print should quote its DOI. When an issue becomes available, queuing Ahead of Print articles will move to that issue's Table of Contents. When the article is published in a journal issue, the full reference should be cited in addition to the DOI.

Downloaded by [University of West London] on [08/08/19]. Copyright © ICE Publishing, all rights reserved.

Accepted manuscript doi:
10.1680/jstbu.19.00081

Submitted: 06 April 2019

Published online in 'accepted manuscript' format: 24 July 2019

Manuscript title: Towards Efficient Structural and Serviceability Design of High-Strength Concrete T-Beams

Authors: Ibrahim G. Shaaban[1] and Tarek S. Mustafa[2]

Affiliations: [1]Civil Engineering and Built Environment, University of West London, UK and [2]Civil Engineering Department, Benha University, Egypt

Corresponding author: Ibrahim G. Shaaban, Civil Engineering and Built Environment, University of West London, UK.

E-mail: ibrahim.shaaban@uwl.ac.uk

Downloaded by [University of West London] on [08/08/19]. Copyright © ICE Publishing, all rights reserved.

Accepted manuscript doi:
10.1680/jstbu.19.00081

Abstract

A total of 10 HSC T-beams having a total length of 1700 mm, web breadth of 100 mm, height of 250 mm, and different flange dimensions, were experimentally tested until failure. The studied parameters were; flange dimensions, transverse reinforcement ratio, and longitudinal reinforcement ratio of the beam. A numerical model was developed to predict the flexural behaviour of the tested beams. The results indicated that increasing breadth, depth, and flange reinforcement ratio led to reduction in the overall deflection, and enhancment of the ultimate load capacity. An empirical equation, developed earlier by the authors for predicting effective moment of inertia for HSC T beams, was used successfully to predict load-deflection relationships for the studied beams. Comparisons were carried out between the load-deflecion curves predicted by the numerical model, those predicted by this equation, and those predicted by Branson equation which is currently used in the design codes. It was found that there was a close agreement between the experimental results, numerical results and those obtained by the authors' equation. This research highlights the need for updating the Branson equation used in the design codes for deflection design of HSC T beams by adopting the equation proposed by the authors.

Keywords: Beams & girders; Codes of practice & standards; Concrete structures; Design methods & aids; High strength concrete

Downloaded by [University of West London] on [08/08/19]. Copyright © ICE Publishing, all rights reserved.

Accepted manuscript doi:
10.1680/jstbu.19.00081

1 INTRODUCTION

The rapid increase in the use of High-Strength Concrete (HSC) in modern construction necessitates additional information on the behaviour of HSC structural elements. Ductility is one of the most important design considerations for HSC structural elements in order to ensure warnings prior to failure. Low ductility of HSC is considered a serious drawback in the design of HSC elements. Beams with high levels of ductility undergo significant deformations in case of a structural failure, which is crucial for the safety of the inhabitants and for the redistribution of loads in the structure (Aykac et al., 2013). In international codes, such as ACI building code (ACI 318-14, 2014) and Eurocode 2 (CEN, 2002), the shear force in a T-beam is assumed to be carried only by the web. Previous studies have shown that the shear strength of a T-beam is, in many cases, considerably higher than that of the rectangular beams of the same web dimensions (Giaccio et al., 2006; Tureyen et al., 2006; Zararis et al., 2006). Seraj et al. (1992) carried out three-dimensional finite-element modelling of normal and high strength reinforced concrete T-beams and they showed that the later type of concrete is even more amenable to simple modelling of complex reinforcement detailing.

Aykac et al. (2013) reported that flexural strengthening of RC T-beams with perforated steel plates, which contributes to the flexure strength, similar to changing the longitudinal steel ratio in the current research, affected the ductility of strengthened beam and changed the mode of failure to pure flexure. You et al. (2017) found that reducing the stirrups spacing from 150 mm to 100 mm resulted in an increase in the diagonal cracking load for T-beams without changing the mode of failure. Cladera et al. (2015) concluded that increasing the flange breadth led to higher positions of neutral axis for predicting the shear–flexural strength of slender reinforced concrete T shaped beams. The first author of this research started studying the behaviour of HSC T shaped beams in 2003. Experimental/theoretical flexural and shear strength behaviour of HSC T-beams including steel fibres under axial compression stress was reported by Shaaban, 2003; Shaaban, 2005; Abdelalim, et al., 2007. Recently, the authors studied the effect of flange dimensions on the short-term deflection and effective moment of inertia of NSC and HSC T-beams (Shaaban et al., 2017). Recently, Ayensa et al. (2019) carried out experimental study and finite element modelling to investigate the influence of the flanges' width and thickness on the shear strength of reinforced concrete beams with T-shaped cross section. They recommended distribution of the shear stresses between the web and flange. They also argued that there is a need to derive a design expression for the shear effective flanges' width of T beams.

2 RESEARCH SIGNIFICANCE

The current research explores the possibility of including the whole section of T-Beam in the analysis and design; hopefully leading to more efficient design of HSC T-beams. In the current research, beside the flange dimensions, the parameters were transverse reinforcement ratios in flange and web, and the longitudinal reinforcement ratio in the web. The crack patterns and mode of failure, load-deflection and ultimate capacity, strains in stirrups and concrete strain distribution were used to evaluate the strength behaviour of the experimentally studied beams. In addition, finite element model was developed to predict the experimental crack pattern and load-deflection relationships. Moreover, the empirical equations proposed earlier by the authors, for predicting effective moment of inertia, were used to predict the load-deflection curves. Comparisons were carried out with experimental results and those predicted by the Branson equation currently used by the design codes in order to propose a more efficient approach to the design of HSC T beams.

Downloaded by [University of West London] on [08/08/19]. Copyright © ICE Publishing, all rights reserved.

Accepted manuscript doi:
10.1680/jstbu.19.00081

3 EXPERIMENTAL PROGRAM

Ten HSC T-shaped simply supported beams of web breadth, 100 mm, total height of 250 mm, clear span of 1500 mm, total length of 1700 mm and of different flange dimensions were experimentally tested under one midspan concentrated static applied load. The shear span-to-depth ratio (a/d), of the studied beams, was kept constant as 3.33 to to concentrate more on the flexural behaviour of the beams (Li and Leung, 2016). Dimensions and details of the tested beams are shown in Figure 1. The compressive strength of the mix for test beams was 70 MPa. Cube compressive strength results at 28 days for studied specimens are reported in Table 1. The studied parameters were the flange breadth and depth, transverse reinforcement ratio in the web and flange, and the longitudinal reinforcement ratio in the web. Table 1 shows the different test beams and the details of the studied parameters.

3.1 Materials

Table 2 provides the mix proportions for the concrete used in this study. Natural sand and two different sizes of basalt (14 and 5 mm) were blended to obtain well-graded aggregates. A superplasticizer based on polynaphthalene sulphate was used to improve the workability of the concrete mix. Ten percent by weight of the portland cement was replaced by silica fume to produce concrete of target strength 70 MPa. The beam specimens were poured in wooden forms along with three standard cubes 150 mm * 150 mm * 150 mm per/beam. The beam specimens and standard cubes were cured in water bath for 28 days before testing. The average actual compressive strength is 72 Mpa. Two types of reinforcing steel were used in this work, namely, high-grade steel (400/600) of diameters 10 mm and 16 mm (designated as H10 and H16), for the longitudinal reinforcement and mild steel (240/350) of diameters 6 mm and 8 mm (designated as H6 and H8), for web/flange reinforcement (stirrups) and top flange reinforcement, (see Figure 1). Reinforcement of each diameter were tested in direct tension to compare their actual mechanical properties with ECP 203-2007 specification. The results of the direct tension test, such as yield strength and ultimate strength, are shown in Table 3.

3.2 Instrumentation and Test Setup

The beams were tested using a 500-ton universal-testing machine, with a computer controlled hydraulic servo system. Figure (2.a) shows the setup of a typical test beam. The locations of the demec points for measuring concrete strains and dial gauges for measuring mid-span deflection are also shown in Figure (2.a). Each beam was tested as a simply supported beam under one vertical concentrated load using a vertical hydraulic jack. An incremental vertical load was applied in 20 KN increments. After each increment, concrete strains were measured using a 150 mm demountable digital demec gauge. The deflections at mid-span have been

Downloaded by [University of West London] on [08/08/19]. Copyright © ICE Publishing, all rights reserved.

Accepted manuscript doi:
10.1680/jstbu.19.00081

measured using dial gauges with 0.01 mm divisions attached to the bottom surface of the test beams as shown in Figure (2.a). The strains in the stirrups were measured using electrical strain gauges of length 5 mm, resistance 120.4 ± 0.4 ohm, and a gauge factor of 2.11. The strain gauges were placed in the stirrups in the critical shear zones as indicated in ECP 203-2007; CEN, 2002; ACI 318-14, 2014 (see Figure 2.b). The strains in the stirrups were measured using P3500 Strain Indicator, Switch & Balance Unit as shown in Figure (2.b). To avoid stress concentration during testing, a steel loading plate of dimensions 200 mm * 300 mm and thickness of 20 mm was placed on top of the beam underneath the loading cell, and steel bearing plates of dimensions 100 mm * 300mm and thickness of 20 mm were placed at the bottom of the beam above the end supports. All beams were statically tested to failure in a single load cycle. Detection and marking of cracks for each incremental load were made when the load reached its steady state.

4 RESULTS AND DISCUSSION

The measured experimental values of the flexural cracking load, diagonal cracking load, ultimate load capacity, and maximum mid-span deflection are recorded in Table 4. Figure (3) shows the crack pattern of the tested beams until failure and the observed failure mode. Figures (4 to 7) shows the effect of flange breadth and thickness, spacing between stirrups in flange and web, and main longitudinal reinforcement in the web on the load-deflection behaviour and load-stirrup's strain relationships. Concrete strain distribution for beams of different flange breadths is shown in Figure (8).

4.1 Crack Pattern and Failure Mode

Figure 3 shows that the first crack for all studied beams occurred in the flexural region perpendicular to the direction of the maximum principal stress induced by pure moment. The shear stresses increased with increasing the load increment and started to induce diagonal cracks. The cracks start to propagate, spread and widen due to the effect of combined shear and bending stresses. Approaching the failure load level, shear cracks started from the support and propagated diagonally towards the point load. At failure load, both of the flexural cracks and the diagonal shear cracks spread into small cracks in the lower third of the beam web as shown in Figure 3. Similar observations were highlighted by Kahn and Slapkus (2004); Abdelalim et al. (2007); Al-Hassani et al. (2015); Halicka and Jabonski (2016); You et al. (2017); González and Ruiz (2017); Shaaban et al. (2017); Ayensa et al. (2019) for normal strength concrete (NSC), Medium Strength Concrete (MSC) and HSC T-beams. It is worth mentioning that most of the failure modes for the test beams were flexure with small contribution of shear stresses as a result of providing relatively high value of shear span-to-depth ratio (a/d) = 3.33.

4.1.1 Effect of flange dimensions

Figure 3 and Table 4 show that increasing flange breadth (B) resulted in more crack concentration at the flexural region and increased the ultimate load with a pure flexure failure mode for beam B2. It was observed that the cracks continued from the web to the bottom of the flange without crushing the flange until beam failure. Table 4 reports that increasing (t_f/t) resulted in increasing the first shear crack load without changing the failure mode. As shown in Table 4 and Figure 3, increasing the flange thickness from 50 mm (t_f/t = 0.2) for beam B3 to 100 mm (t_f/t = 0.4) for beam B4 resulted in increasing the first diagonal cracking load by 37.5% while the failure mode was still flexural failure. Figure 3 also shows minor cracks in

Downloaded by [University of West London] on [08/08/19]. Copyright © ICE Publishing, all rights reserved.

Accepted manuscript doi:
10.1680/jstbu.19.00081

the beam B3 that continued to the bottom of the flange in the region of the flexural cracks without occurring damage in the flange. Similar observations were found by You et al. (2017), who reported that changing the flange size affected the first shear crack load in the experimental study of shear behaviour of hybrid-fiber-reinforced self-compacting concrete T-beams.

4.1.2 Effect of transverse and longitudinal steel

The analysis of the results provided in Table 4 showed that reducing the main longitudinal reinforcement from 2H16 for beam B7 to 2H10 for beam B8, resulted in increasing the number of flexural cracks, without a significant change in the failure mode. Reducing the same amount of main longitudinal reinforcement for beams of higher flange thickness (as in beams B4 to B9), resulted in a better behaviour in terms of reducing cracks compared to that of beam B8 and the failure mode was still pure flexure (see Table 4 and Figure 3). Carpinteri et al. (2014) reported also that the longitudinal steel ratio and the flange thickness for T beams have a reasonable effect on the ductility of these beams. Increasing the transverse reinforcement ratio resulted in a reduction in the cracks spacing and crack width, an increase in the number of cracks, and an increase in the first diagonal cracking load, while the failure mode was still flexure. For Beam B7 with spacing between stirrups of 200 mm, the diagonal cracking load was 40 KN and the failure mode was flexure at the middle third of the beam. Reducing the spacing between stirrups to 150 mm for beam B5 led to increasing the first shear crack load to 60 KN as shown in Table 4. Reducing spacing between stirrups to 100 mm for beam B6 resulted in a further increase in the first shear crack load to 70 KN. This is in agreement with Arun et al. (2013) who reported the effect of changing stirrups' spacing on the diagonal cracking load and shear strength of HSC T-beams.

4.2 Load-Deflection Behaviour

The load-deflection relationships for all the test beams with different flange breadths, thicknesses, different shear reinforcement ratios and different main longitudinal reinforcement are shown in Figures (4) and (5).

4.2.1 Effect of flange dimensions

Figure (4.a) shows the effect of flange breadth on the load-deflection relationships of test beams with similar flange thicknesses and similar reinforcement. It can be seen from the figure that increasing the flange breadth led to an increase in the ultimate load of the test beams and a reduction of the overall deflection. The ultimate load for the rectangular control beam (B10) is 100 kN at a maximum deflection of 3.35 mm while the overall deflection for the T-beam of flange breadth equals 200 mm (B1) is 3.25 mm only at the same load level (100 kN). The increase in the ultimate load of beam B1 was 20% when compared to the rectangular control beam B10. Increasing the flange breadth to 400 mm for beam B7 led to an increase in the ultimate load by 23% over that of the rectangular beam B10. A further increase in the flange breadth of 600 mm for beam B2 resulted in an increase of 27% in the ultimate load and 25% reduction in the maximum deflection when compared to the rectangular beam B1. Similar gains in the ultimate load and the reduction in the overall deflection were observed by Halicka and Jabonski (2016) in the study of MSC composite T-beams.

Figure (4.b) shows the effect of flange thickness on the load-deflection relationships for the studied beams of the same flange breadth and flange reinforcement. It can be

Downloaded by [University of West London] on [08/08/19]. Copyright © ICE Publishing, all rights reserved.

Accepted manuscript doi:
10.1680/jstbu.19.00081

seen from the figure that increasing the flange thickness led to a reduction in the overall deflection and enhancement of the ultimate load. Increasing the flange thickness to 75 mm for the beam B7 resulted in an increase of 12% in the ultimate load capacity and 13% reduction in the maximum deflection when compared to beam B3 with flange thickness of 50 mm. The increase in the ultimate load capacity and the reduction in the overall deflection for the beam B4 with a flange thickness of 100 mm were 16% and 31%, respectively, when compared to beam B3. Similar observations were found by Ayensa et al. (2019) when they studied the effect of flange dimensions on reinforced concrete T-beams. Higher observed values in the ultimate loads and reduction of overall deflection were reported by You et al. (2017) as a result of increasing the flange thickness. This may be attributed to the effect of adding fibers in their study, which improved the behaviour of the test beams compared to the test beams in the current study.

4.2.2 Effect of transverse and longitudinal reinforcement

Figure (5.a) shows the effect of reducing the amount of main longitudinal reinforcement for beams of different flange thicknesses on the load-deflection relationship. It can be seen from the figure that increasing the amount of the longitudinal reinforcement led to an increase in the ultimate load and a decrease in the overall deflection. Compared to beam B7 with longitudinal reinforcement of 2H16, beam B8 with longitudinal reinforcement 2H10 showed a reduction in the ultimate load by 39% and an increase in the overall deflection by 34% while all other variables were kept constant. On the other hand, beam B9 with longitudinal reinforcement of 2H10 showed a reduction of 27% in the ultimate load capacity when compared to beam B4 with longitudinal reinforcement of value 2H16. This is in agreement with the findings of Thamrin et al. (2016), where the ratio of longitudinal reinforcement influences the shear capacity of the beam as well as the angle of diagonal shear crack. It has been noted that the general behaviour of beam B9 is almost similar to that of beam B3. This indicates that the effect of reducing the flange thickness from 100 mm to 50 mm on the ductility of the studied beams was almost similar to reducing the main longitudinal reinforcement from 2H16 to 2H10.

The effect of changing the spacing between stirrups in flange and web reinforcement on the load-deflection relationship is shown in Figure (5.b). Reducing the spacing between stirrups to 150 mm (beam B5) led to an increase in the ultimate load and a reduction in the overall deflection by 6.0% and 10%, respectively, when compared to beam B7 with stirrups spacing of 200 mm. A further reduction of the spacing between stirrups to 100 mm for beam B6 resulted in a further increase in the ultimate load and a reduction in the overall deflection to 12% and 17%, respectively, when compared to beam B7. This shows that the flange and web reinforcement affects the flexural behaviour of the studied beams.

4.3 Strain in the Stirrups

The effect of the studied experimental parameters on the load-stirrup strain relationships is shown in Figures (6 and 7). It can be seen from the figures that, generally, the strain in the stirrups were increasing very slowly with increasing the applied load until the cracks reached the considered stirrup. With increasing the applied loads, the strain increased rapidly with different values.

Downloaded by [University of West London] on [08/08/19]. Copyright © ICE Publishing, all rights reserved.

Accepted manuscript doi:
10.1680/jstbu.19.00081

4.3.1 Effect of flange dimensions

Figure 6 shows that the strain for the control rectangular beam, B10 increased very rapidly starting from load level of 70 KN until the ultimate load at strain value of $1.65 * 10^{-3}$. Figure (6.a) shows that the stirrup's strain at the ultimate load level for the T-beam, B1, reduced by 6% only. Increasing the flange breadth from 200 mm for Beam B1 to 400 mm for Beam B7 led to a reduction in the stirrup's strain by 35% with a slight increase in the ultimate load by 2.5%. Figure 6(b) shows that increasing the flange thickness from 50 mm for beam B3 to 75 mm for beam B7 resulted in a reduction of 33% in the maximum stirrup's strain. Further increase in the flange thickness to 100 mm for beam B4 led to a reduction in the stirrup strain by 45% when compared to beam B3. It was noticed that the rate of increase in the strains for Beam B4 was rapid up to a certain point, beyond which it became slower. This drop in the rate of increase in the strains was also observed by Ahmad et al. (1995), for HSC and NSC tested beams. It was attributed to the slippage in parts of the stirrups. It can be noticed from the above discussion that the effect of flange thickness, transverse and longitudinal reinforcement, were more significant than that of the flange breadth on the strains of the stirrups.

4.3.2 Effect of transverse and longitudinal reinforcement

The effect of transverse reinforcement ratio in the flange and web is shown in Figure 7(a). It can be seen from the figure that increasing reinforcement ratio by reducing the spacing between stirrups led to a reduction in the stirrups' strains and an enhancement of the ultimate load capacity because of stirrups' contribution in resisting shear stresses. Beam B6 with the smallest spacing between stirrups of 100 mm showed a reduction in the strains of the stirrups by 43% when compared to beam B7 with spacing between stirrups of 200 mm. It can be argued that the strains in the stirrups were higher when a diagonal crack crossed the stirrups, because the diagonal crack can be considered as a yield line. Hamrat et al. (2012) found similar observations indicating the significance of transverse reinforcement on the shear capacity and ductility of HSC beams. The effect of reducing longitudinal reinforcement ratio, for beams of different flange thicknesses, on the stirrups' strain in the critical shear zone is shown in Figure 7(b). It can be seen from the figure that reducing the longitudinal reinforcement from 2H16 for beam B7 to 2H10 for beam B8 led to an increase in the stirrup's strain by 52%. Reducing the same amount of reinforcement for a beam of higher flange thickness (Beam B9) resulted in an increase of stirrup's strain also by 52%. Additionally, the test beam with the minimum spacing between stirrups (Beam B6) had the best behaviour among the studied beams in terms of shear strain in stirrups. It can be argued that the stirrup strain measurements can be used as indicators of the contribution of stirrup reinforcement at critical shear zones. It should be pointed out that the strain values reported in this investigation are not necessarily maximum values. They are strictly related to the location of the gages with respect to that of the shear cracks.

4.4 Concrete Strain Distribution

Figure 8 shows the strain distribution results across the flange and web section at the demec points shown in Figure 2 for the first crack load, working load (65% of the ultimate load) and ultimate load for three test beams of different flange breadths (200 mm, 400 mm and 600 mm). The strain distribution curves intersected together to locate the position of the neutral axis at a specific distance measured from the bottom of the beam. This distance changed with changing the flange breadth. It can be seen from Figure 8 that the tensile strains were much higher than the compressive strains and the strain distribution was almost linear across the

Downloaded by [University of West London] on [08/08/19]. Copyright © ICE Publishing, all rights reserved.

Accepted manuscript doi:
10.1680/jstbu.19.00081

beam depth due to the ductile behaviour of the beams as the tensile reinforcement reached its yield strength. Figure 8 shows also that the maximum strains at failure loads for the selected test beams were between 0.0012 to 0.002. It can be seen from the figure that increasing the flange breadth led to a reduction of the maximum concrete strain at the tension zone and a higher position of the neutral axis measured from the bottom of the beam. Figure 8 shows also that, for the three test beams that have different flange breadths, B2 had a maximum strain of 0.0012 at a maximum ultimate load of 127 KN. The maximum concrete strains for beams B1 and B7 were 0.002 and 0.00175 at maximum ultimate loads of 120 KN and 123 KN, respectively. The ratios of the ultimate concrete strains to the concrete strains at first cracking loads, for the beams B1, B2 and B7 were 207%, 300%, and 246%, respectively. These high ratios indicates an increase in ductility with enlarging the flange breadth, in line with the findings observed earlier for the load-deflection relationships. Similar to the observations in the current research, Cladera et al. (2015) concluded that increasing the flange breadth led to a higher position of neutral axis for predicting the shear–flexural strength of slender reinforced concrete T shaped beams.

5 FINITE ELEMENT PREDICTION FOR LOAD DEFLECTION OF TEST BEAMS

The nonlinear finite element program; ANSYS 12 (ANSYS®, 2009) was used to predict the behaviour of the tested beams. A correlative study based on the load- deflection response as well as the cracking patterns was conducted to verify the numerical model with the obtained experimental results. Based on the theoretical manual of ANSYS program, a brief description is given here for the finite element modeling of concrete and steel for RC element.

5.1 Finite Element Discretization and Solution Technique

The SOLID65 element was employed for discretizing concrete matrix in the tested beams. It is defined by eight nodal points as shown in Figure 9. The element is capable of directional integration point cracking in tension and crushing in compression. In the present work, tested beams were typically discretezeid using average mesh of size 50 * 50 * 50 mm solid elements. The flexural and shear reinforcement in the tested beams were idealized using the Link8 element as shown in Figure 10. The axial stress is assumed to be uniform over the entire element. Full bond was assumed between concrete and reinforcing steel. Both linear and non-linear behaviours of the concrete were considered. For the linear stage, the concrete is assumed to be an isotropic material up to cracking. For the non-linear segment, the concrete may undergo plasticity. The numerical solution scheme adopted for non-linear

Downloaded by [University of West London] on [08/08/19]. Copyright © ICE Publishing, all rights reserved.

Accepted manuscript doi:
10.1680/jstbu.19.00081

analysis was an incremental load procedure based on the iterative solution using Newton-Raphson method. The convergence criterion currently used was based on the iterative nodal displacement where only transitional degrees of freedom were considered.

5.2 Constitutive Modeling for Concrete

The concrete material model assigned for Solid65 element used throughout this study is characterized by its capability to predict the failure of brittle materials. Both cracking and crushing failure modes are accounted for. The criterion for failure of concrete due to a multi-axial stress state can be expressed in the form:

$$\frac{F}{f_c} - S \geq 0 \qquad (1)$$

To model concrete behaviour, nonlinear stress-strain curves were used in compression and tension (Montoya et al., 2001). Such models account for compression & tension softening, tension stiffening and shear transfer mechanisms in cracked concrete as presented in Figure 11.

5.3 Constitutive Modeling for Steel

The average stress-strain curve developed earlier by Soroushian and Lee (1989) for steel bars embedded in concrete is used in the current research (see Figure 12). The stress-strain relationship is expressed by two straight lines as follows:

For $\varepsilon_s \leq \varepsilon_n$:

$$f_s = E_s \varepsilon_s \qquad (2)$$

and for $\varepsilon_s \geq \varepsilon_n$:

$$f_s = f_y \left[(0.91 - 2B) + \left(0.02 + 0.25B \frac{\varepsilon_s}{\varepsilon_y} \right) \right] \qquad (3)$$

Downloaded by [University of West London] on [08/08/19]. Copyright © ICE Publishing, all rights reserved.

Accepted manuscript doi:
10.1680/jstbu.19.00081

Where $\varepsilon_n = \varepsilon_y (0.93 - 2B)$.

And the parameter B is given as $\left(f_{cr} / f_y \right)^{1.5} / \rho$

The recommended value of f_{cr} is given as:

$$f_{cr} = 0.31\sqrt{f_c^{/}} \qquad \text{In MPa} \qquad (4)$$

5.4 Finite Element Model of the Tested Beams

In the finite element discretization of each beam, a mesh of average size 50 * 50 * 50 mm of eight-node elements was used for all beams. The area and spacing of bar elements were similar to the experimental specimens. The concentrated load was also applied to the top surface at mid-span of the tested beams. The supports were represented by restrained nodes at the corresponding locations. The initial Young's modulus in concrete has been considered as 41 GPa; and the steel modulus as 200 GPa. Figures 13 and 14 show the typical idealization of the concrete and steel elements for the tested beams used in the analysis.

5.5 Simulation of Cracking Patterns

The computed cracking patterns at different loading levels are presented for the tested beams B1, B2, B5, B7, B8 and B10 as shown in Figure 15. Similar to the experimetal observations, The shear stresses increases with increasing the load increment and starts to induce diagonal cracks. The cracks start to propagate, spread and widen due to the effect of combined shear and bending stresses at average load level of 50%. At failure load, both of the flexural cracks and the diagonal shear cracks spread into small cracks in the lower third of the beam web as observed in the experimental cracking patterns. There is a good agreement between the simulated crack patterns and the obtained experimental ones. The simulation also successfully predicted the sequence in the crack patterns development and the failure mechanism.

Downloaded by [University of West London] on [08/08/19]. Copyright © ICE Publishing, all rights reserved.

Accepted manuscript doi:
10.1680/jstbu.19.00081

5.6 Predicted Load-Deflection Curves

In Figure 16, test results of load- deflection curves are compared to the predictions of finite element analysis for the tested beams for the tested beams B1, B2, B5, B7, B8 and B10. A good agreement between the experimental and finite element results was obtained at different levels. In simulated curves, there is a sudden increase in the deflection and this is attributed to formation of the first flexural crack. Similar to experimental results, simulated curves are significantly affected by the flange dimensions and flexural reinforcement. It can be seen from Figure 16 that increasing the flange breadth led to an increase in the ultimate load of the test beams and a reduction of the overall deflection. Additionally, increasing the amount of the longitudinal reinforcement led to an increase in the ultimate load and a decrease in the overall deflection. All studied beams exhibited different displacement ductility at failure, indicated by the are under the load-deflection curve. The degree of ductility varied depending on the flange dimensions and the flexural reinforcement ratio where the lower flange dimesnions or the larger reinforcement ratio, the lower is the amount of ductility. Increasing either vertical or horizontal shear reinforcement led to an increase in the analytical load carrying capacity and ductility matching with the experimental results.

6 EMPIRICAL EQUATION FOR PREDICTION OF LOAD DEFLECTION RELATIONSHIP OF T-BEAMS

The effective moment of inertia for reinforced concrete beams is usually calculated by Branson's equation (Branson, 1963). This equation is adopted in all international design codes (ACI 318-14, 2014; Eurocode 2, CEN, 2002):

$$I_e = (M_{cr(exp)} / M_a)^3 I_g + [1 - (M_{cr(exp)} / M_a)^3] I_{cr} \leq I_g \qquad (5)$$

Al-Shaikh and Al-Zaid (1993) further improved Branson's Equation (5) for better prediction of effective moment of inertia by converting it to a general form:

$$I_e = (M_{cr(exp)} / M_a)^m I_g + [1 - (M_{cr(exp)} / M_a)^m] I_{cr} \leq I_g \qquad (6)$$

Earlier, Shaaban et al. (2017) proved that Branson's equation was not accurate for predicting the effective moment of inertia for HSC T beams. They modified the equation proposed by Al-Shaikh and Al-Zaid (1993) to be applicable for HSC highly reinforced T-beams by modifying the value of ρ in the exponent "m" by curve fitting for several experimentally tested beams in their research and from literature as follows:

$$m = 3.0 - 1.4\rho \qquad (7)$$

Downloaded by [University of West London] on [08/08/19]. Copyright © ICE Publishing, all rights reserved.

Accepted manuscript doi:
10.1680/jstbu.19.00081

The effective deflection at different load levels can be calculated based on the elastic deflection theory by substituting I_e from Equation (5) (Branson's equation) or substituting I_e from Equation (6) as proposed by Al-Shaik and Al-Zaid (1993) and Equation (7) as proposed by the authors (Shaaban et al., 2017):

$$\Delta = k\, P_{exp}\, L^3 / (E_c\, I_e) \quad (8)$$

Based on the previous equations, the load-deflection curves for the test beams B1, B2, B5, B7, B8 and B10 can be predicted. At different experimental load levels and up to the ultimate load, the corresponding deflections have been calculated using Equation (8). Finally, the load-deflections curves predicted based on the Branson's equation, by applying Equations (5 & 8) or by the authors proposed equations, by applying Equations (6, 7 & 8), were plotted and compared with the experimental and the finite element load-deflection curves (see Figure 16). It can be seen from Figure 16 that the load-deflection relations predicted by the authors proposed equations were in very good agreement with the experimental curves and finite element prediction. However, the load deflection relationships predicted by Branson's equation did not correlate well with any of these curves. It is interesting to find that the authors proposed empirical equations were in a better agreement with experimental results compared to the finite element prediction in some of the studied beams such as B8 and B10 (see Figure 16). This highlights the need for revision of the current design codes when applied to design HSC T beams. It is recommended that the authors proposed equations are added to the current design codes and utilized for the design of HSC T beams.

7 CONCLUSIONS

The experimental and theoretical prediction of flexural strength of HSC T-shaped beams have been studied in this research. The following conclusive points were drawn based on this study:

1. Increasing the flange dimensions (breadth and/or thickness) led to a general improvement of the flexural behaviour of the test beams as reflected by the increase in the ultimate load capacity, a reduction in the stirrups' strain and overall deflection to different degrees and, in some cases, changing the failure mode of the tested beams.
2. Increasing the flange breadth led to a reduction of the maximum concrete strain at tension zone and a higher position of the neutral axis measured from the bottom of the beam. This indicates an increase in ductility with enlarging the flange breadth. The finding is in line with similar observations reported in the literature.
3. The effect of increasing the flange thickness from 50 mm to 100 mm on the ultimate load and corresponding deflection of the test beams is almost similar to increasing the main longitudinal reinforcement from 2H10 to 2H16. This indicates that the flange thickness has a significant effect on the flexural behaviour of the test beams.
4. The predictions of load-deflection response as well as the cracking patterns using the nonlinear finite element program, ANSYS 12, showed good agreement with the experimental results. The developed finite element model

Downloaded by [University of West London] on [08/08/19]. Copyright © ICE Publishing, all rights reserved.

Accepted manuscript doi:
10.1680/jstbu.19.00081

predicted successfully the ultimate loads, displacement ductility and failure mechanisms for the test beams with different variables.

5. The authors proposed empirical equations predicted the load deflection response, based on calculated effective moment of inertia, to a higher accuracy compared with Branson equation used in the design codes (ACI Committee 318, 2014; CEN, 2002). The load-deflection curves based on this equation were in a close agreement with the experimental and numerical load deflection relationships.
6. The output of this research highlighted the effect of flange dimensions and reinforcement for T- beams. Based on the proposed empirical equation and the finite element results in this research, it is recommended that the current design codes should be reviewed by adopting the proposed equation for the design of HSC T beams.

ACKNOWLEDGEMENT

Experimental work was carried out in the Reinforced Concrete Testing Laboratory at Cairo University. Professor Akram Torkey, staff and technicians are acknowledged for their great help.

Notation

P_u	Ultimate load
P_{cr}	first flexural cracking load
P_{Dcr}	first diagonal cracking load
w_{max}	maximum overall deflection at ultimate load
f_{cu}	concrete compressive strength
B/b_w	ratio of the total breadth of the flange to the web breadth
t_f/t	ratio of the flange thickness to total beam thickness
F	a function of the principal stress state; σ_{xp}, σ_{yp}, σ_{zp};
S	failure surface expressed in terms of principal stresses and the strength parameters f_t, f_c, f_{cb}, f_1 and f_2
f_t	ultimate uniaxial tensile strength;
f_c	ultimate uniaxial compressive strength;
f_{cb}	ultimate biaxial compressive strength;

Downloaded by [University of West London] on [08/08/19]. Copyright © ICE Publishing, all rights reserved.

Accepted manuscript doi:
10.1680/jstbu.19.00081

f_1	ultimate compressive strength for a state of biaxial compression superimposed on hydrostatic stress state
f_2	ultimate compressive strength for a state of uni-axial compression superimposed on hydrostatic stress state.
f_s and ε_s	the average stress and strain of steel bars, respectively
f_y and ε_y	the yield stress and strain of steel bars, respectively
E_s	the young's modulus of steel reinforcement;
f_{cr}	the cracking strength of concrete.
I_g	the gross moment of inertia for the un-cracked section
I_{cr}	the moment of inertia of the cracked transformed section
$M_{cr\ (exp)}$	the first cracking moment of the beam, calculated from the experimental first crack load at the load-deflection curve
M_a	the maximum service load moment acting on the beam.
m	the experimentally determined exponent for use in the equation
ρ	reinforcement ratio
L	span of the studied beam (1500mm)
E_c	modulus of elasticity of concrete.
k	constant depends on the type of loading and end conditions (k = 1/48 for simply supported beams under a midspan concentrated load).
Δ	maximum deflection

Downloaded by [University of West London] on [08/08/19]. Copyright © ICE Publishing, all rights reserved.

Accepted manuscript doi:
10.1680/jstbu.19.00081

References

Abdelalim, O. A., Ghallab, A. H., Shaaban, I. G., and Elnawawy, O. A., 2007, "Effect of Axial Compression Stress on The Shear Behaviour of High-Strength Fibre Reinforced Concrete T-Beams", Twelfth International Colloquium on Structural and Geotechnical Engineering, ICSGE, Ain Shams University, 10-12 December, Cairo, Egypt.

ACI Committee 318, 2014, " Building Code Requirements for Structural Concrete (ACI 318-14) and Commentary. ACI "American Concrete Institute", 38800 Country Club Drive Farmington Hills, MI 48331 U.S.A.

Ahmad, S. H., Park, F. and El-Dash, K., 1995, "Web Reinforcement Effects on Shear Capacity of Reinforced High-Strength Concrete Beams," Magazine of Concrete Research, Vol. 47, No. 172, Sept., pp. 227-233.

Al-Hassani, H. M., Al-Kafaji, J. M. and Ismael, M. A., 2015, "Flexural Behavior of Hybrid Tee Beams (Containing Reactive Powder Concrete and Normal Strength Concrete)", Journal of Engineering and Development, Vol.19, No.2, March, pp. 123-140, ISSN 1813- 7822.

Al-Shaikh, A. H. and Al-Zaid, R. Z., 1993, Effect of reinforcement ratio on the effective moment of inertia of reinforced concrete beams, ACI Structural Journal, 90(2), pp. 144-149.

ANSYS® (2009) "Engineering Analysis System User's Manual, Vol. 1 & 2, and Theoretical Manual," Revision 13.0, Swanson Analysis System Inc., Houston,Pennsylvania.

Arun, M., Velrajkumar, G., and Ranjith, S., "*Behavior and shear strength of reinforced concrete T-beams with stirrups"* International Journal of Emerging Trends in

Downloaded by [University of West London] on [08/08/19]. Copyright © ICE Publishing, all rights reserved.

Accepted manuscript doi:
10.1680/jstbu.19.00081

Engineering and Development Issue 3, Vol.6 (November 2013), pp. 161-173. http://www.rspublication.com/ijeted/ijeted_index.htm.

Ayensa, A., Oller, E., Beltran, B., Ibarz, E., Mari, A., and Gracia, L., 2019, "Influence of the flanges width and thickness on the shear strength of reinforced concrete beams with T-shaped cross section", Engineering Structures, Vol. 188, pp. 506-518. https://08101zekd-1106-y-https-doi-rg.mplbci.ekb.eg/10.1016/j.engstruct.2019.03.057

Aykac, S., Kalkan, I., Aykac, B., and Ozbek, E., 2013, "Strengthening of RC T-beams with perforated steel plates", Magazine of Concrete Research, Vol. 65, No. 1, pp. 37–51. http://dx.doi.org/10.1680/macr.12.00004.

Bischoff, P. H. and Scanlon, A., 2007, "Effective moment of inertia for calculating deflections of concrete members containing steel reinforcement and fiber-reinforced polymer reinforcement", ACI Structural Journal 104(1): 68-75.

Branson, D. E. Instantaneous and time-dependent deflections of simple and continuous reinforced concrete beams, HPR Report No. 7, Part 1, Alabama Highway Department, Bureau of Public Roads, 1963, pp. 1-78.

Cladera, A., Mari, A., Ribas, C., Bairan, J., and Oller, E., 2015, "Predicting the shear–flexural strength of slender reinforced concrete T and I shaped beams", Engineering Structures, Vol. 101, pp. 386-398.

Carpinteri, A., Cadamuro, E., and Corrado, M., "Minimum flexural reinforcement in rectangular and T-section concrete beams", Structural Concrete 15 (2014), No. 3, pp. 361-372. DOI: 10.1002/suco.201300056.

CEN (2002), European Committee for Standardization, "Eurocode 2: Design of Concrete Structures - Part 1: General Rules and Rules for Buildings", Brussels, pp. 26-35 & 132.

Downloaded by [University of West London] on [08/08/19]. Copyright © ICE Publishing, all rights reserved.

Accepted manuscript doi:
10.1680/jstbu.19.00081

Giaccio, C., Mahaidi, R. A. and Taplin, G., 2006, "Flange strain measurement in shear critical RC T-beams", Advances in Structural Engineering, Vol. 9, No. 4, pp. 491–505.

Halicka, A. and Jabonski, Ł., 2016, "Shear failure mechanism of composite concrete T-shaped beams", Proceedings of the Institution of Civil Engineers, Structures and Buildings, Volume 169, Issue SB1, pp. 67–75 http://dx.doi.org/10.1680/stbu.14.00127

Hamrat, M., Boulekbache, B., Chemrouk, M. and Amziane, S., 2012, "Effects of the Transverse Reinforcement on the Shear Behaviour of High Strength Concrete Beams," Advances in Structural Engineering, Vol. 15, No. 8, pp. 1291-1306.

Kahn, L. F. and Slapkus, A., 2004, "Interface Shear in High Strength Composite T-Beams," PCI Journal, July-August, pp. 102-110.

Kong, P. Y. L. and Rangan, B.V., 1998, "Shear Strength of High-Performance Concrete Beams," ACI Structural Journal, Vol. 95, No. 6, pp. 677-688.

Li, W. and Leung, C. K.Y., "Shear Span–Depth Ratio Effect on Behavior of RC Beam Shear Strengthened with Full-Wrapping FRP Strip", Journal of Composites for Construction, Vol. 20, No. 3, pp. 04015067-1-14, DOI: 10.1061/ (ASCE) CC.1943-5614.0000627.

Ribas-González, C. R. and Fernández-Ruiz, M. F., 2017, "Influence of flanges on the shear-carrying capacity of reinforced concrete beams without web reinforcement," International Federation for Structural Concrete, Structural Concrete, pp. 1–13, DOI: 10.1002/suco.201600172.

Seraj, S.M., Kotsovos, M.D., and Pavolovics, 1992, "Three-Dimensional Finite-Element Modelling of Normal and High-Strength Reinforced Concrete Members, with Special Reference to T-Beams", Computers & Structures, Vol. 44, No. 4, pp. 669-716.

Downloaded by [University of West London] on [08/08/19]. Copyright © ICE Publishing, all rights reserved.

Accepted manuscript doi:
10.1680/jstbu.19.00081

Shaaban, I. G., 2003, "Effect of Flange Characteristics on the Behaviour of High-Strength Concrete T-Beams," Journal of the Egyptian Society of Engineers, Vol. 42, No. 2, April-June, pp. 13-24.

Shaaban, I. G., 2005, "Effect of axial force and fibre type on the shear behaviour of high strength fibre reinforced concrete beams," International Conference on Cement Combinations for Durable Concrete, Dundee, Scotland, 5-7 July. DOI: 10.1680/ccfdc.34013.0056.

Shaaban, I. G., Saidani, M., Nuruddin, M.F., Malkawi, A. and Mustafa, T.S., 2017, "Serviceability Behaviour of Normal and High-Strength Reinforced Concrete T-Beams", European Journal of Materials Science and Engineering (EJMSE) www.ejmse.tuiasi.ro, ISSN: 2537-4338, Volume 2, Issue 4, pp. 99-110. http://www.ejmse.tuiasi.ro/articles/EJMSE_02_04_01_Shaaban.pdf.

Soroushian, P. and Lee, C-D, "Constitutive Modeling of Steel Fiber Reinforced Concrete under Direct Tension and Compression", Fiber Reinforced Cements and Concrete: Recent Developments. Proceedings of an International Conference held at the University of Wales, College of Cardiff, School of Engineering, UK, Sep. 18-20, 1989, pp. 363-377.

Thamrin, R., Tanjung, J., Aryanti, R., Nur, O. F., and Devinus, A., 2016, "Shear Strength of Reinforced Concrete T-Beams without Stirrups" Journal of Engineering Science and Technology, Vol. 11, No. 4, pp. 548 – 562.

You, Z., Wang, X., Liu, G., Chen, H., and Li, S., 2017, "Shear behaviour of hybrid fibre-reinforced SCC T-beams", Magazine of Concrete Research, Volume 69 Issue 18, pp. 919-938, http://dx.doi.org/10.1680/jmacr.16.00470.

Downloaded by [University of West London] on [08/08/19]. Copyright © ICE Publishing, all rights reserved.

Accepted manuscript doi:
10.1680/jstbu.19.00081

Zararis, L. P., Karaveziroglou, M. K. and Zararis, P. D., 2006, "Shear strength of reinforced concrete T-beams". ACI Structural Journal, Vol. 103, No. 5, pp. 693–670.

Table 1 Layout of the Test Beam Specimens

Test beam designation	Actual Concrete Compressive Strength (MPa)	Flange Dimensions, mm		B/b_w	t_f/t	Web/Flange Reinforcement (Stirrups)	Main Reinforcement
		Breadth (B)	Thickness (t_f)				
B1	76	200	75	2	0.3	H8/6@200-mm	2H16
B2	74	600	75	6	0.3	H8/6@200-mm	2H16
B3	74	400	50	4	0.2	H8/6@200-mm	2H16
B4	72	400	100	4	0.4	H8/6@200-mm	2H16
B5	70	400	75	4	0.3	H8/6@150-mm	2H16
B6	70	400	75	4	0.3	H8/6@100-mm	2H16
B7	70	400	75	4	0.3	H8/6@200-mm	2H16
B8	71	400	75	4	0.3	H8/6@200-mm	2H10
B9	70	400	100	4	0.4	H8/6@200-mm	2H10
B10	75	----	----	---	---	H8/6@200-mm	2H16

Table 2 Mix Proportions of HST T-shaped Beams

Target Strength, 70 MPa	Solid constituents and proportions, kg/m^3				Liquids, Liter/ m^3	
	Cement	Sand	Crushed Basalt	Silica Fume	Water	Superplasticizer
	540	530	1125	60	157	23

Downloaded by [University of West London] on [08/08/19]. Copyright © ICE Publishing, all rights reserved.

Accepted manuscript doi:
10.1680/jstbu.19.00081

Table 3 Mechanical properties of tested reinforcement and specification

Property	ECP 203-2007 Specification		Test Results			
			H6	H8	H10	H16
Diameter (mm)			6	8	10	16
Grade	240/350	400/600	240/350		400/600	
Shape	plain	deformed	plain		deformed	
Yield stress (N/mm^2)	Min 240	Min 400	301	311	418	424
Ultimate stress (N/mm^2)	Min 350	Min 600	406	432	726	738
Weight per meter length (kg)	-	-	0.22	0.395	0.621	1.58

Table 4 Cracking loads, ultimate loads and mid-span deflection of the tested beams

Test beam designation	f_{cu} MPa	t_f/t	B/b_w	P_{cr}: KN	P_{Dcr}: KN	P_u: KN	w_{max}, mm
B1	76	0.3	2	20	40	120	3.25
B2	74	0.3	6	30	40	127	3.41
B3	74	0.2	4	25	40	110	3.25
B4	72	0.4	4	20	55	127	3.25
B5	70	0.3	4	25	60	130	3.36
B6	70	0.3	4	17.5	70	138	3.72
B7	70	0.3	4	20	40	123	3.35
B8	71	0.3	4	20	38	75	3.90
B9	70	0.4	4	20	40	93	3.90
B10	75	---	---	30	50	100	3.35

Downloaded by [University of West London] on [08/08/19]. Copyright © ICE Publishing, all rights reserved.

Accepted manuscript doi:
10.1680/jstbu.19.00081

Figure captions

Figure 1 Dimensions and details of the test beams (a) Locations of demec points and dial gauges on a typical test beam, (b) Measuring strains in stirrups using switch & balance unit

Figure 2 Setup of a typical test beam

Figure 3 Crack pattern and failure mode for different studied beams. (a) Effect of flange breadth, (b) Effect of flange thickness

Figure 4 Effect of flange dimensions on the load-deflection behaviour of test beams. (a) Effect of longitudinal reinforcement, (b) Effect of flange and web transverse reinforcement

Figure 5 Effect of transverse and longitudinal reinforcement on the load-deflection behaviour of test beams. (a) Effect of flange breadth, (b) Effect of flange thickness

Figure 6 Effect of flange dimensions on the load-stirrups' strain relationships for test beams. (a) Effect of flange and web transverse reinforcement, (b) Effect of longitudinal reinforcement

Figure 7 Effect of transverse and longitudinal reinforcement on the load-stirrups' strain relationships for the test beams.

Figure 8 Concrete strain distribution for test beams.

Figure 9 Geometry of 3-D Solid 65 Element (ANSYS®, 2009)

Figure 10 Link8-Element (ANSYS®, 2009)

Figure 11 Stress-strain curve for concrete (Montoya et al., 2001)

Figure 12 Stress-strain curve for steel reinforcement (Soroushian and Lee, 1989)

Figure 13 Typical Idealization of the Tested Beams for Concrete Element.

Figure 14 Typical Idealization of Tested Beams for Steel Element

Figure 15 Simulated crack propagation for selective test beams

Downloaded by [University of West London] on [08/08/19]. Copyright © ICE Publishing, all rights reserved.

Accepted manuscript doi:
10.1680/jstbu.19.00081

Figure 16 Comparisons between experimental and predicted load-deflection curves for selective beams

Downloaded by [University of West London] on [08/08/19]. Copyright © ICE Publishing, all rights reserved.

Accepted manuscript doi:
10.1680/jstbu.19.00081

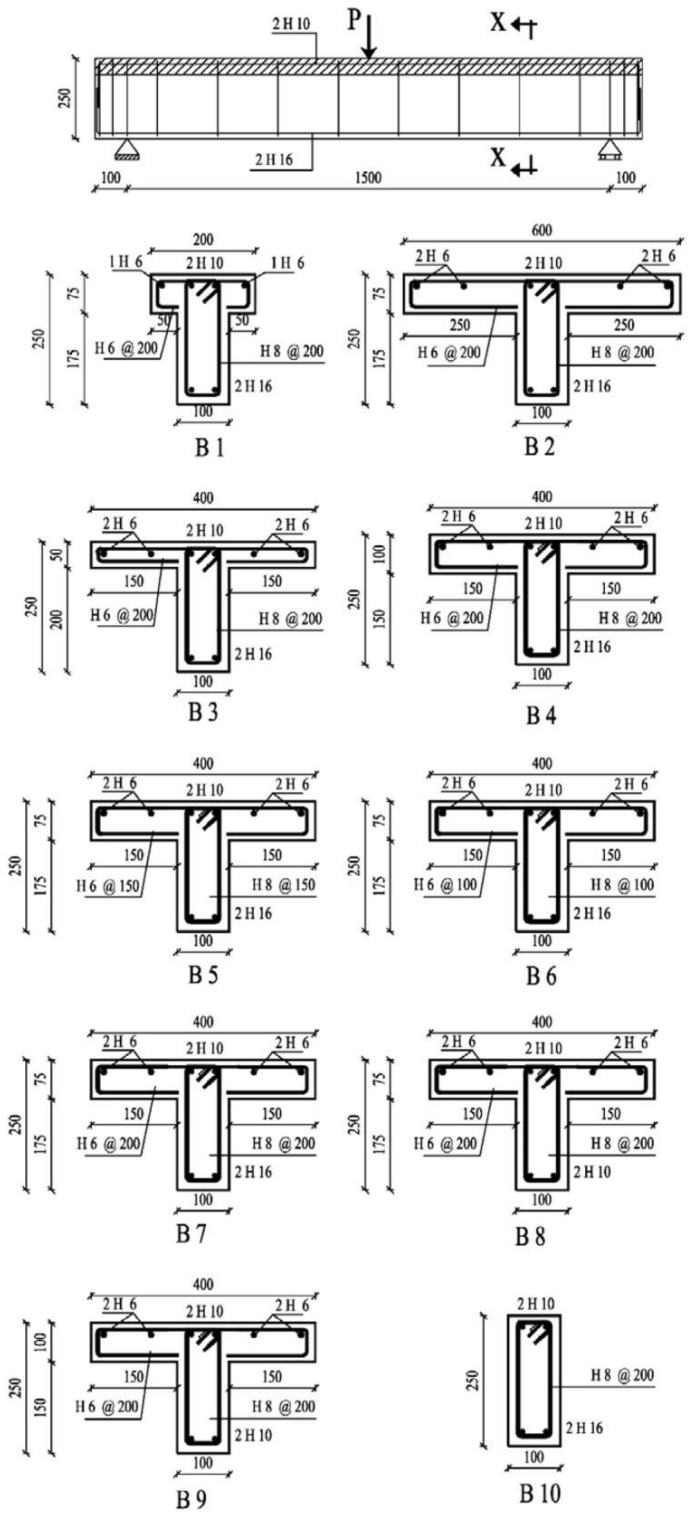

Fig. 1.jpg

Downloaded by [University of West London] on [08/08/19]. Copyright © ICE Publishing, all rights reserved.

Accepted manuscript doi:
10.1680/jstbu.19.00081

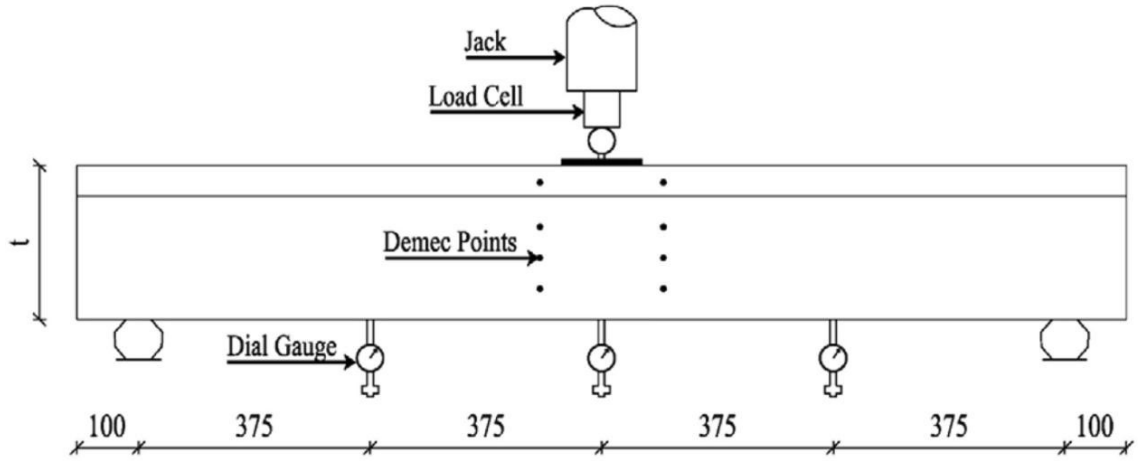

a

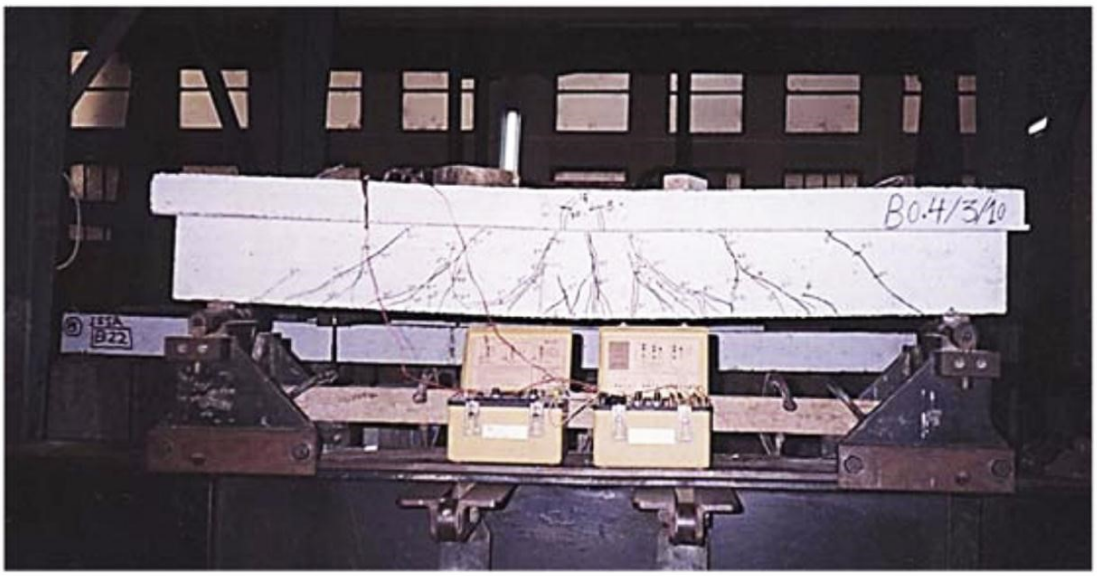

b

Fig. 2.jpg

Downloaded by [University of West London] on [08/08/19]. Copyright © ICE Publishing, all rights reserved.

Accepted manuscript doi:
10.1680/jstbu.19.00081

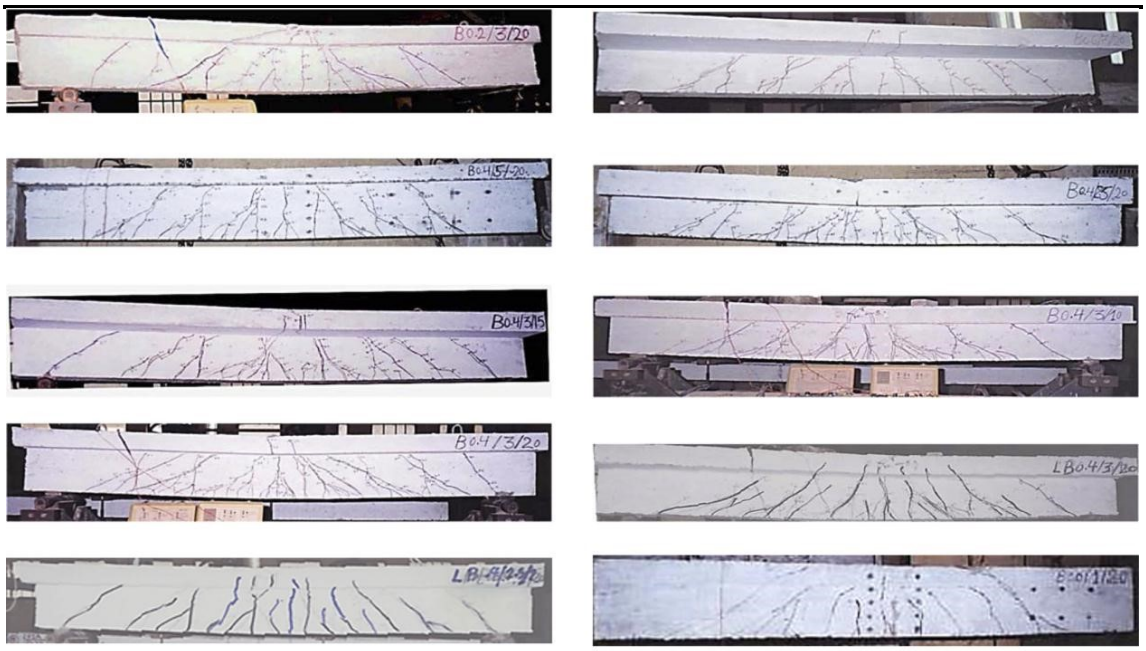

figure3.jpg

Downloaded by [University of West London] on [08/08/19]. Copyright © ICE Publishing, all rights reserved.

Accepted manuscript doi:
10.1680/jstbu.19.00081

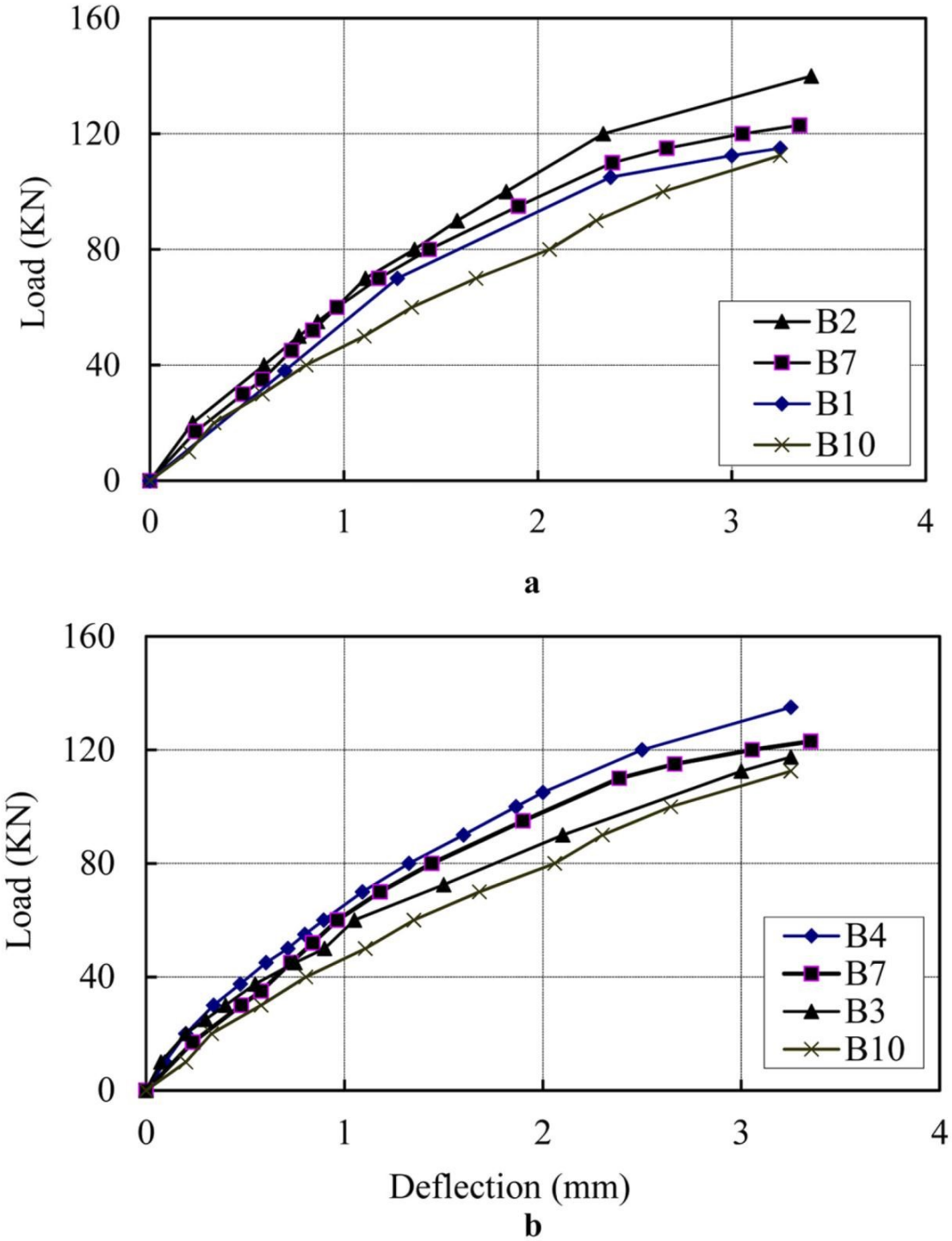

Fig. 4.jpg

Downloaded by [University of West London] on [08/08/19]. Copyright © ICE Publishing, all rights reserved.

Accepted manuscript doi:
10.1680/jstbu.19.00081

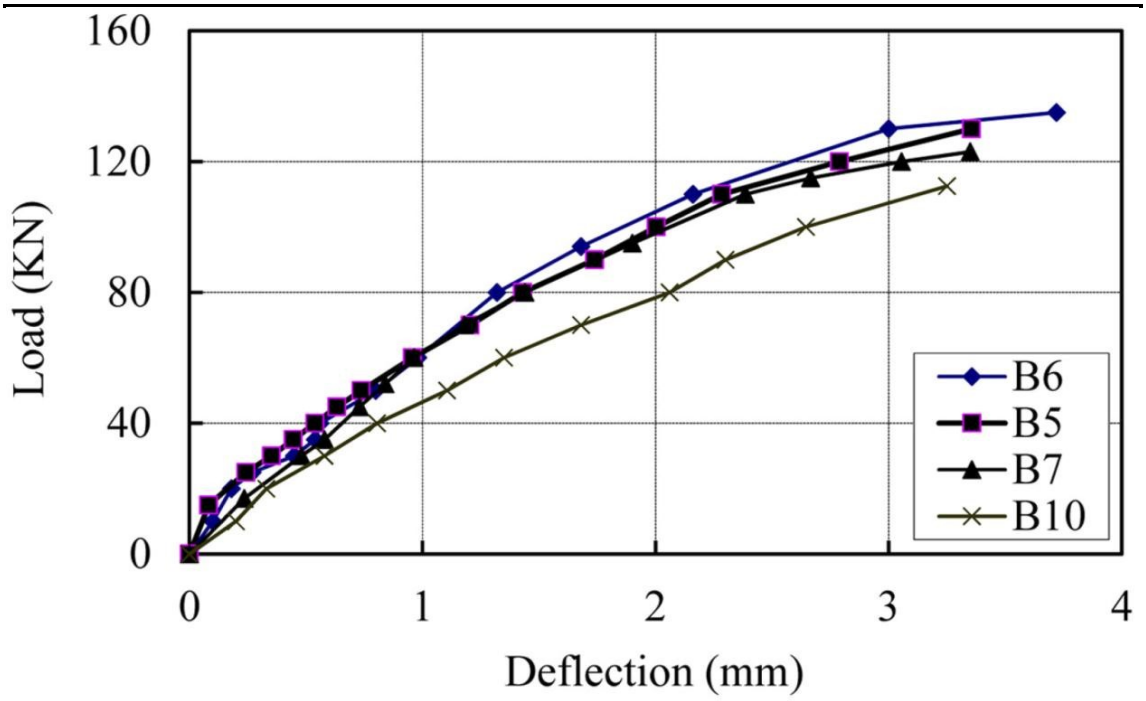

Fig. 5a.jpg

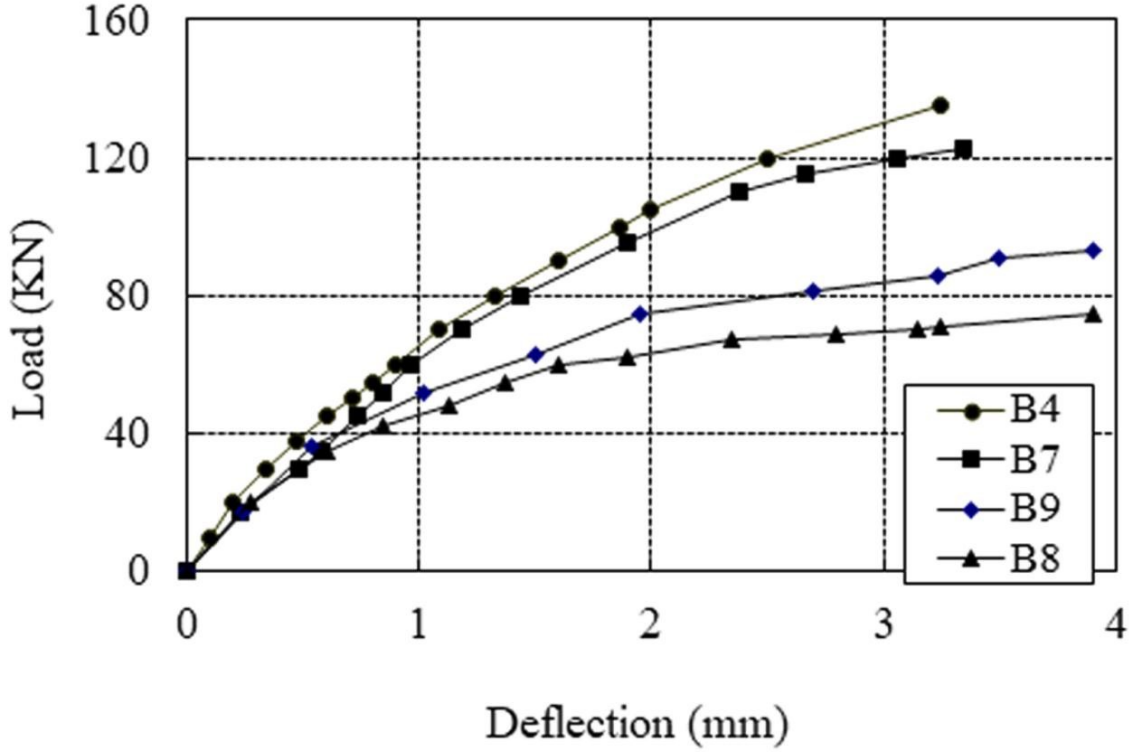

Fig. 5b.jpg

Downloaded by [University of West London] on [08/08/19]. Copyright © ICE Publishing, all rights reserved.

Accepted manuscript doi:
10.1680/jstbu.19.00081

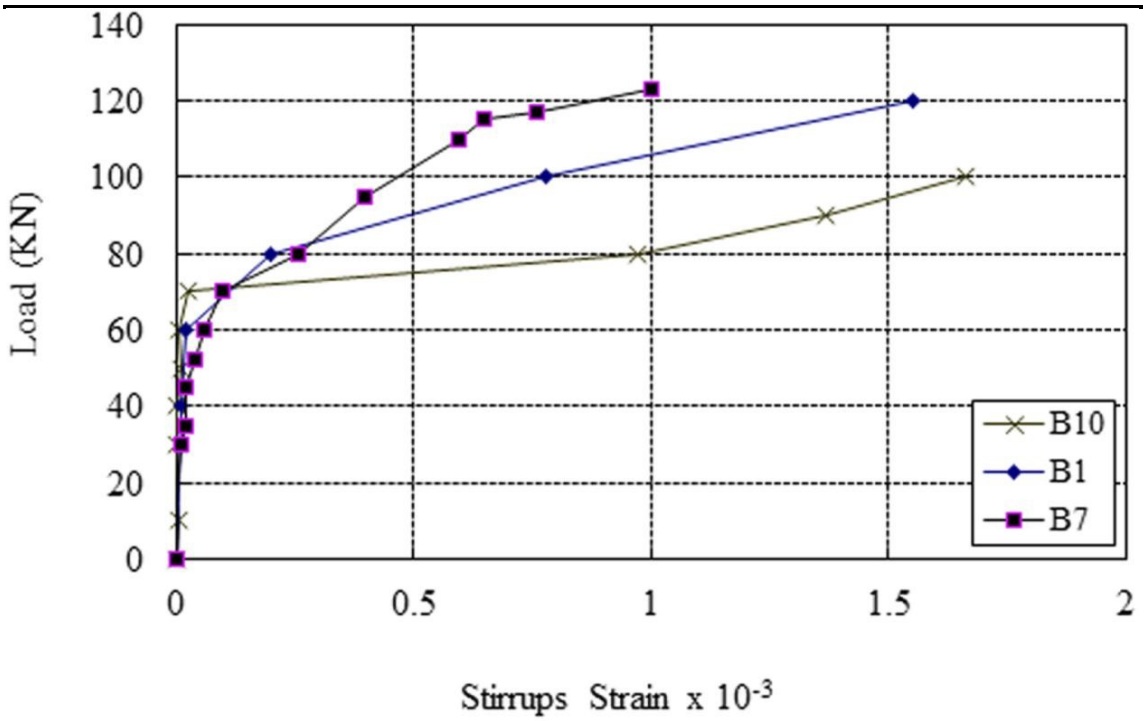

Fig. 6a.jpg

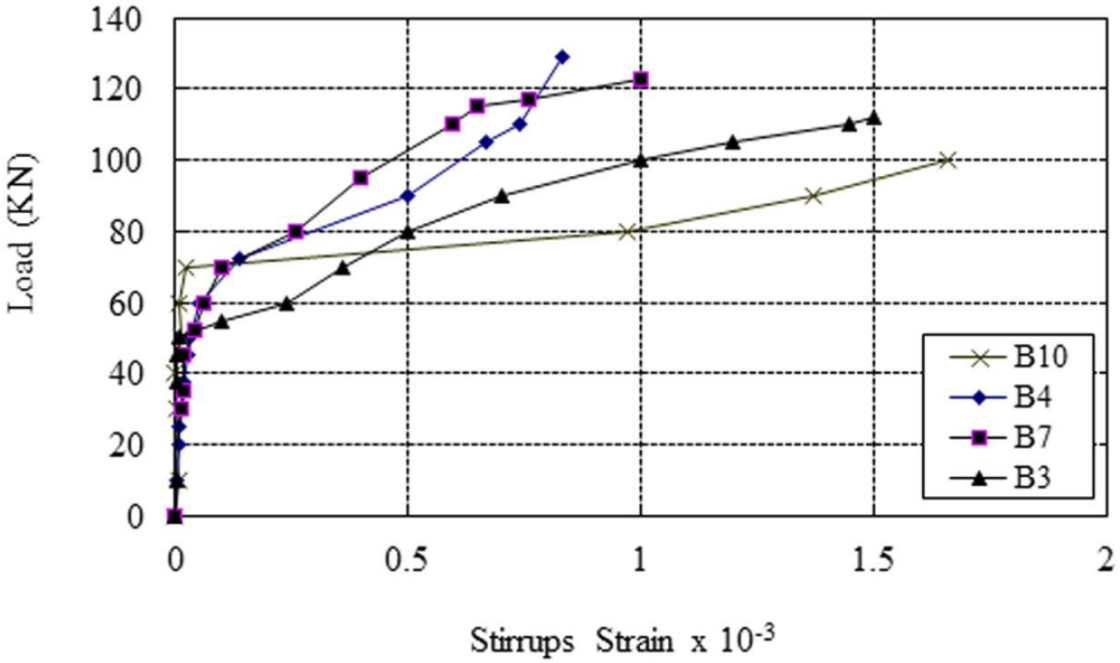

Fig. 6b.jpg

Downloaded by [University of West London] on [08/08/19]. Copyright © ICE Publishing, all rights reserved.

Accepted manuscript doi:
10.1680/jstbu.19.00081

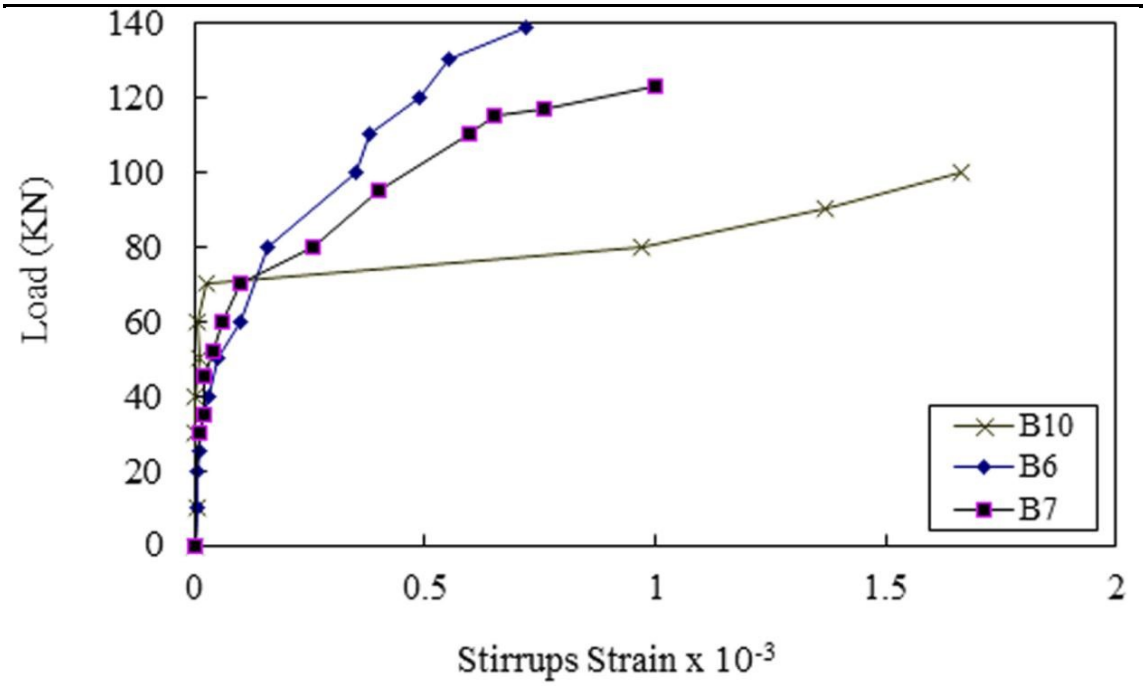

Fig. 7a.jpg

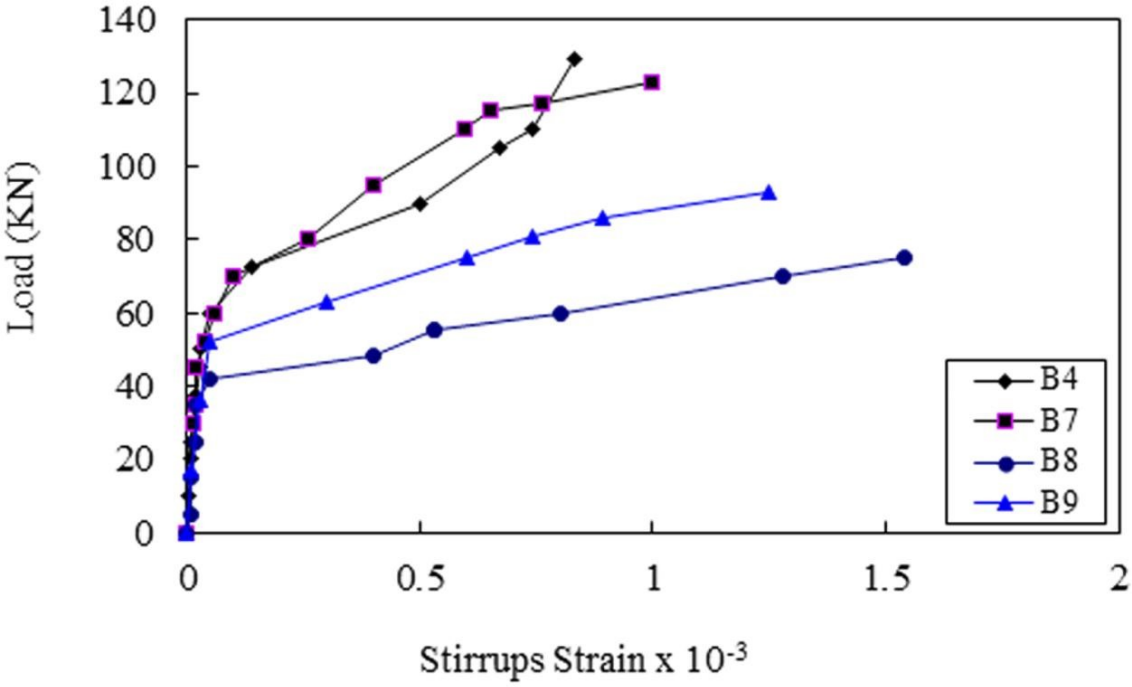

Fig. 7b.jpg

Downloaded by [University of West London] on [08/08/19]. Copyright © ICE Publishing, all rights reserved.

Accepted manuscript doi:
10.1680/jstbu.19.00081

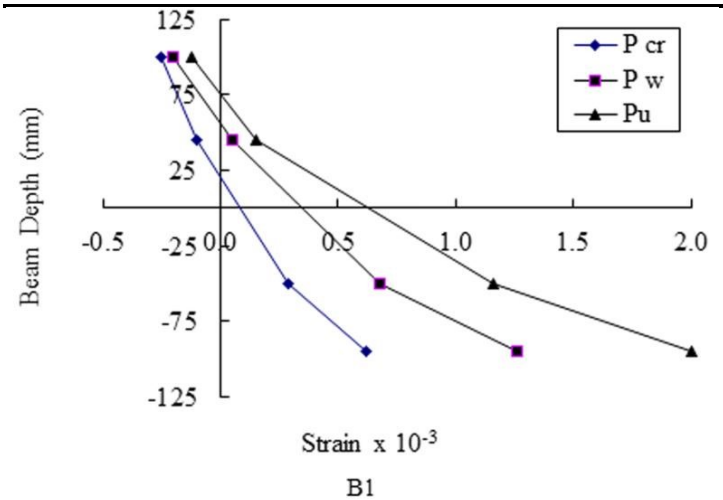

Fig. 8 (B=200mm).jpg

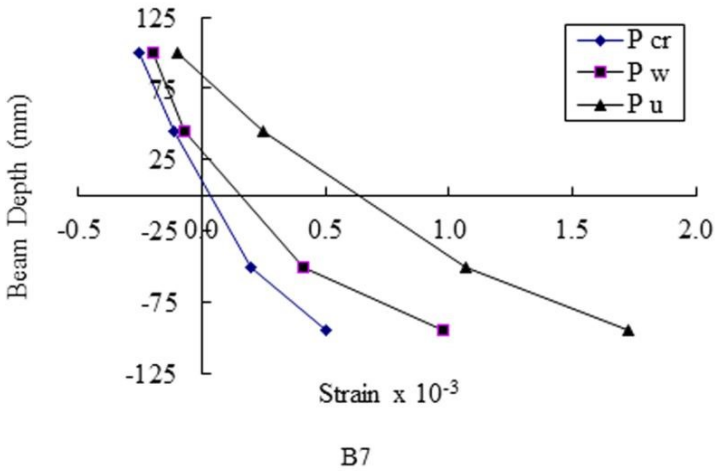

Fig. 8 (B=400mm).jpg

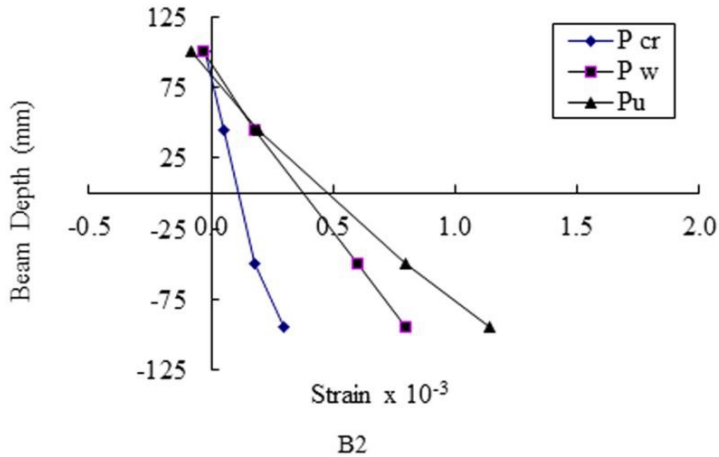

Fig. 8 (B=600mm).jpg

Downloaded by [University of West London] on [08/08/19]. Copyright © ICE Publishing, all rights reserved.

Accepted manuscript doi:
10.1680/jstbu.19.00081

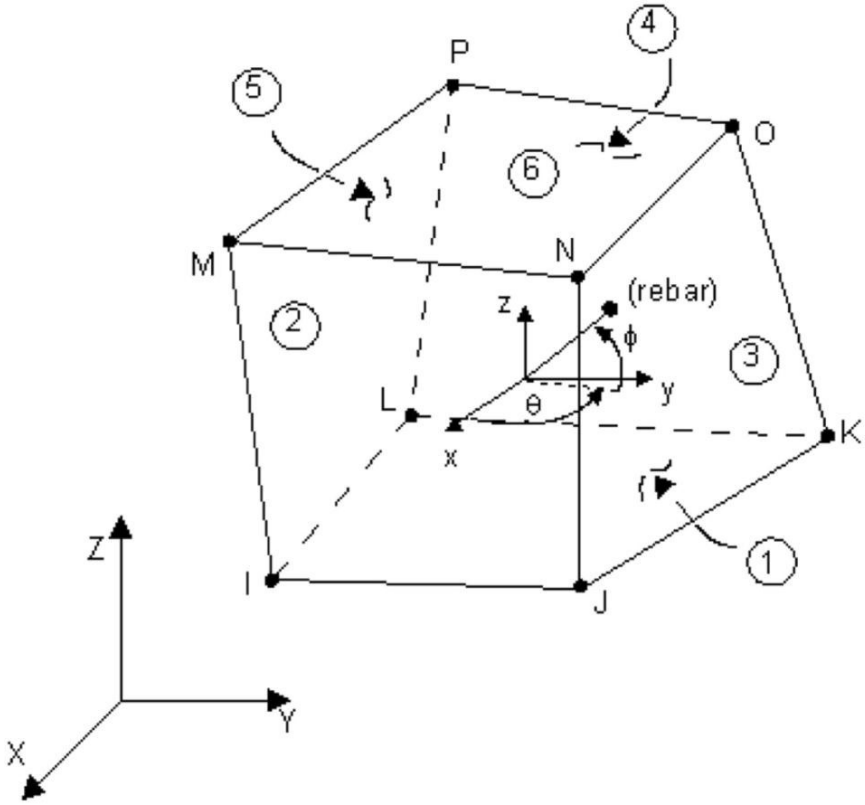

Fig. 9.jpg

Downloaded by [University of West London] on [08/08/19]. Copyright © ICE Publishing, all rights reserved.

Accepted manuscript doi:
10.1680/jstbu.19.00081

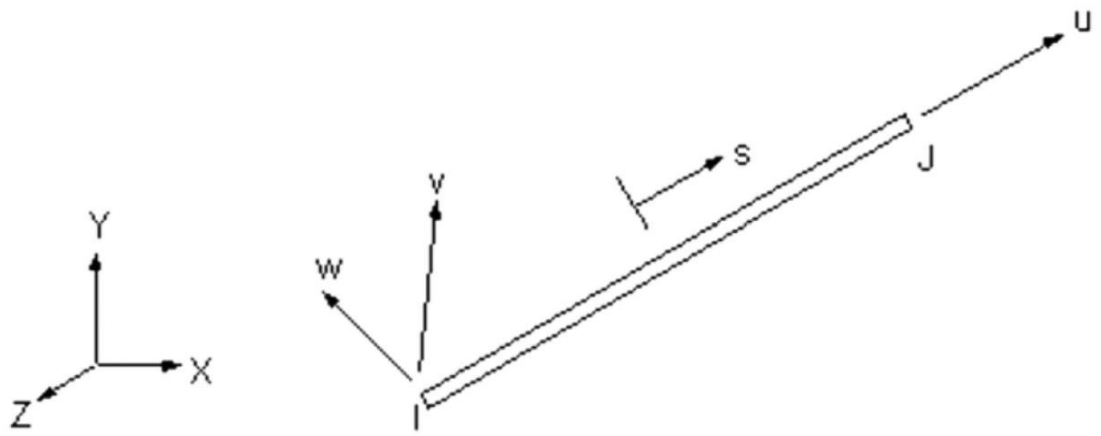

Fig. 10.jpg

Downloaded by [University of West London] on [08/08/19]. Copyright © ICE Publishing, all rights reserved.

Accepted manuscript doi:
10.1680/jstbu.19.00081

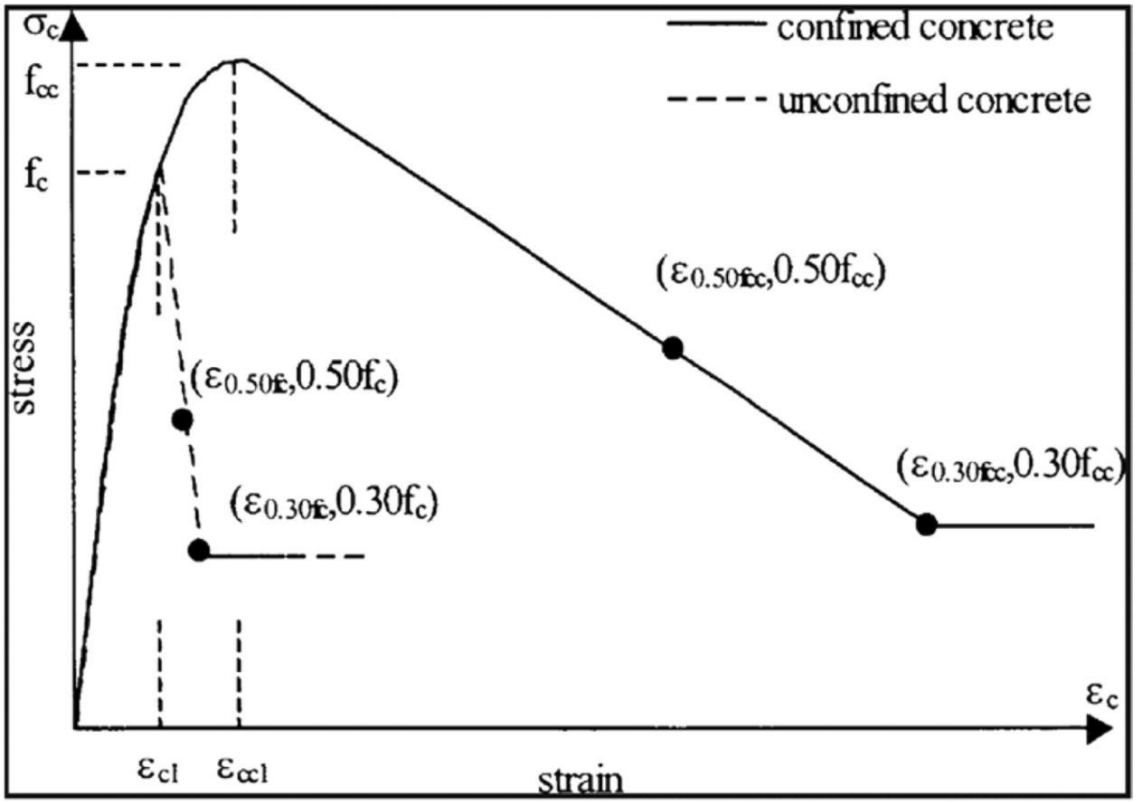

Fig. 11.jpg

Downloaded by [University of West London] on [08/08/19]. Copyright © ICE Publishing, all rights reserved.

Accepted manuscript doi:
10.1680/jstbu.19.00081

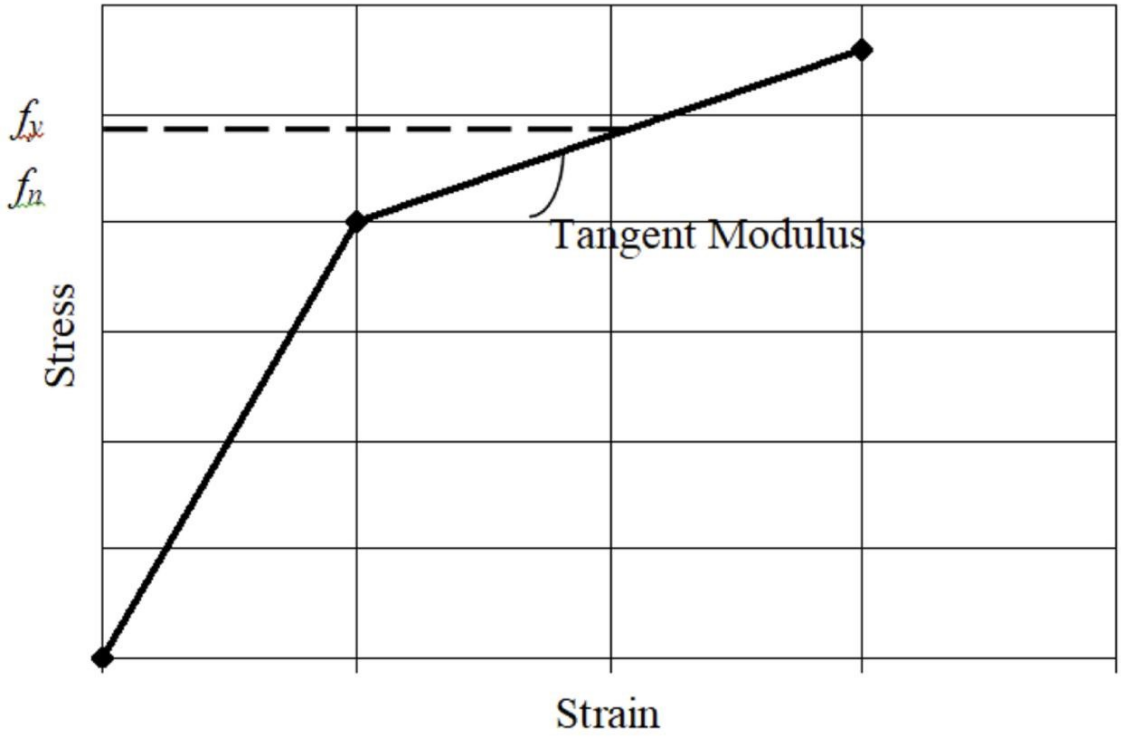

Fig. 12.jpg

Downloaded by [University of West London] on [08/08/19]. Copyright © ICE Publishing, all rights reserved.

Accepted manuscript doi:
10.1680/jstbu.19.00081

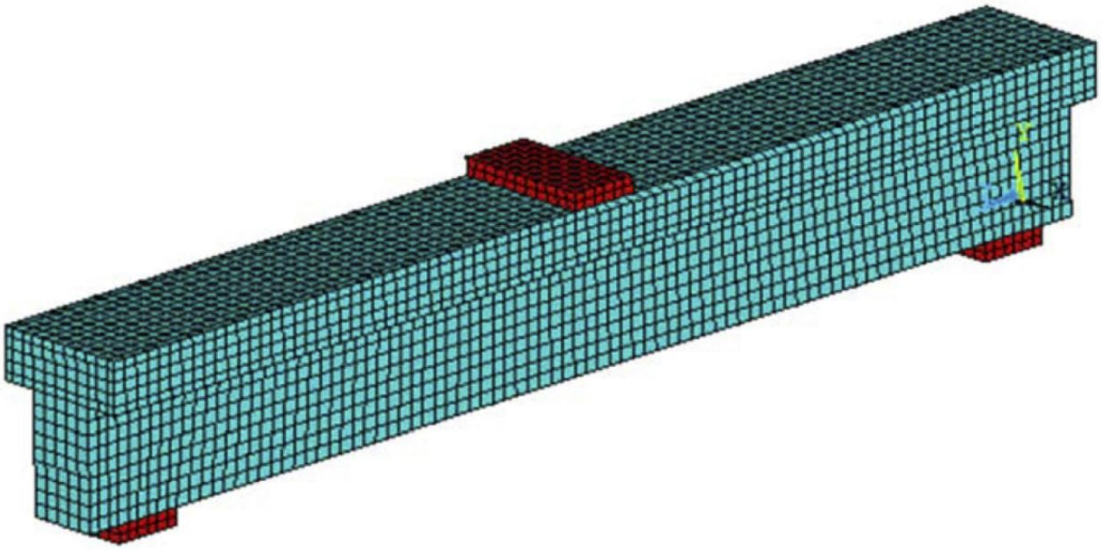

Fig. 13.jpg

Downloaded by [University of West London] on [08/08/19]. Copyright © ICE Publishing, all rights reserved.

Accepted manuscript doi:
10.1680/jstbu.19.00081

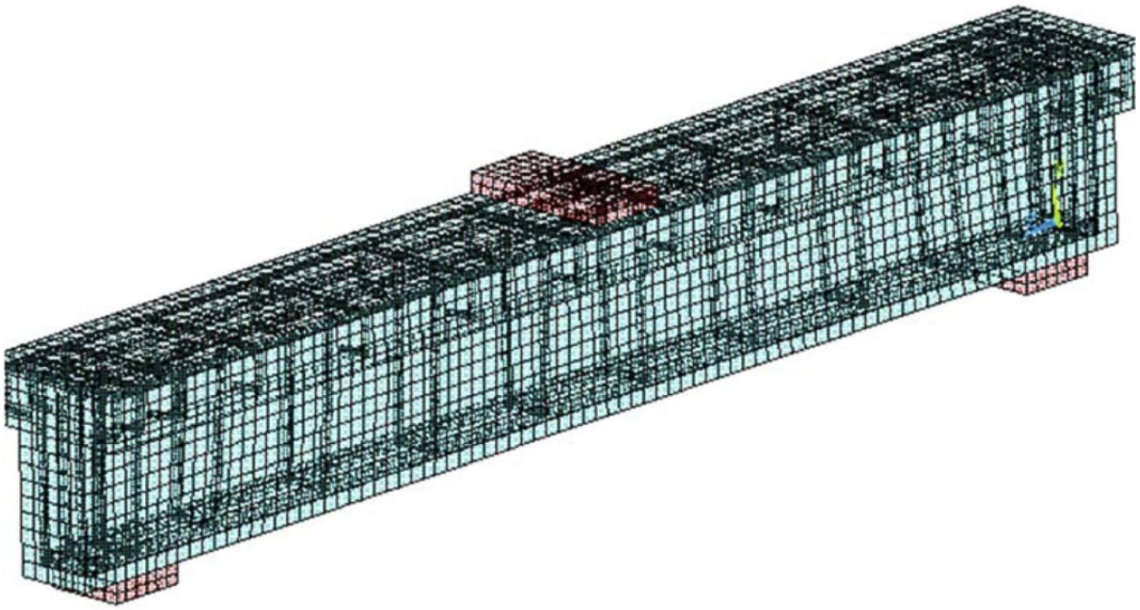

Fig. 14.jpg

Downloaded by [University of West London] on [08/08/19]. Copyright © ICE Publishing, all rights reserved.

Accepted manuscript doi:
10.1680/jstbu.19.00081

Fig. 15 (B1).jpg

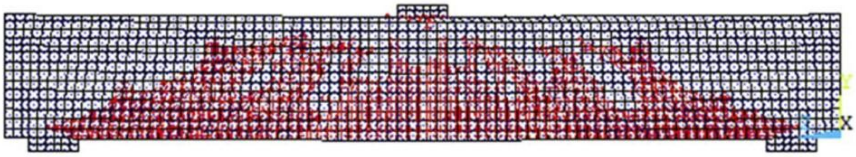

Fig. 15 (B10).jpg

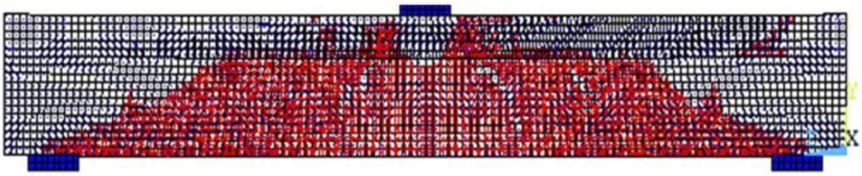

Fig. 15 (B2).jpg

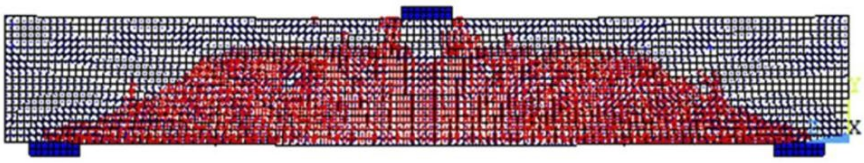

Fig. 15 (B5).jpg

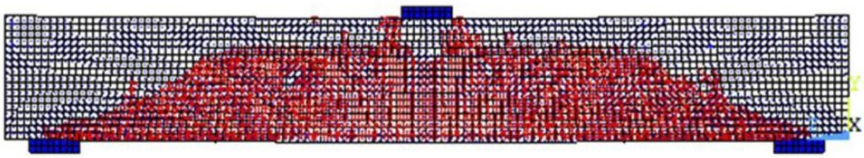

Fig. 15 (B7).jpg

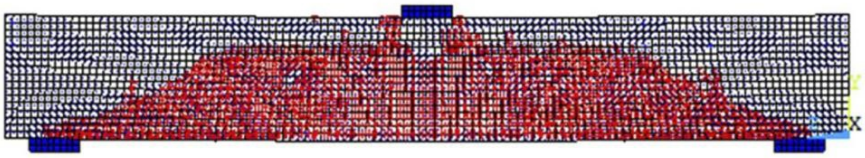

Fig. 15 (B8).jpg

Downloaded by [University of West London] on [08/08/19]. Copyright © ICE Publishing, all rights reserved.

Accepted manuscript doi:
10.1680/jstbu.19.00081

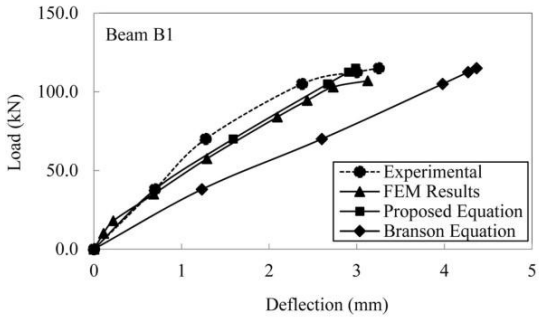

Fig. 16 (B1).jpg

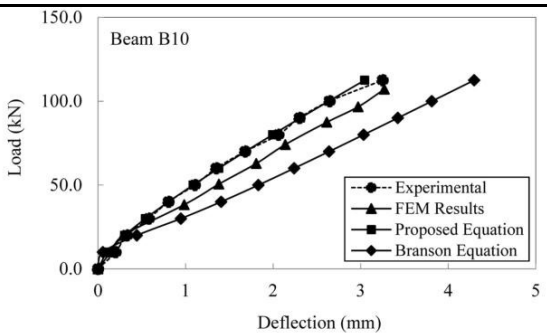

Fig. 16 (B10).jpg

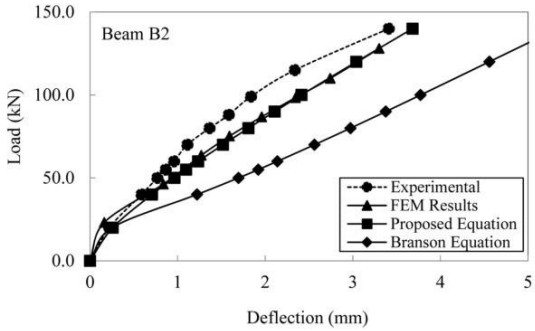

Fig. 16 (B2).jpg

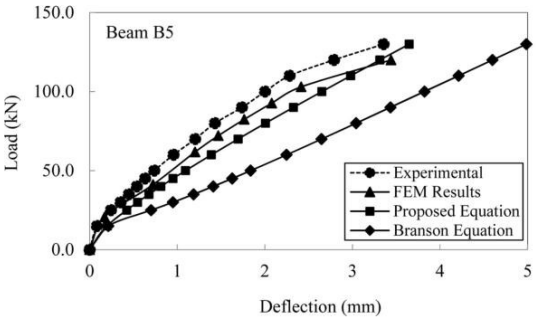

Fig. 16 (B5).jpg

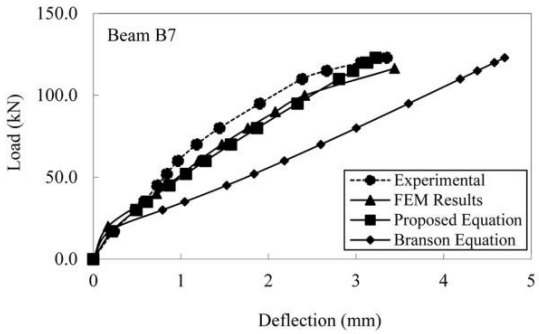

Fig. 16 (B7).jpg

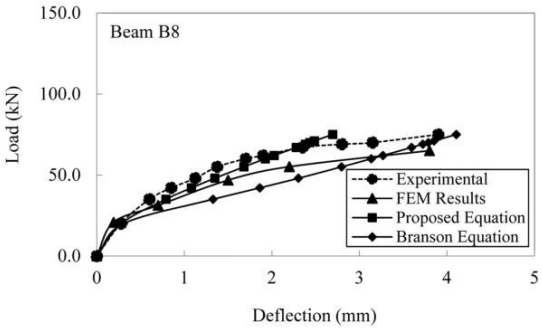

Fig. 16 (B8).jpg

Downloaded by [University of West London] on [08/08/19]. Copyright © ICE Publishing, all rights reserved.